

Received 20 April 2021; revised 8 October 2021; accepted 23 October 2021.  
Date of publication 15 November 2021; date of current version 3 December 2021.

Digital Object Identifier 10.1109/JTEHM.2021.3128276

# Development of an Instrument to Assess the Stability of Cementless Femoral Implants Using Vibration Analysis During Total Hip Arthroplasty

STEVEN LEURIDAN<sup>1</sup>, QUENTIN GOOSSENS<sup>1</sup>, LEONARD CEZAR PASTRAV<sup>1</sup>,  
MICHIEL MULIER<sup>2</sup>, WIM DESMET<sup>3</sup>, JOS VANDER SLOTEN<sup>1</sup>, AND KATHLEEN DENIS<sup>1</sup>

<sup>1</sup>KU Leuven, Department of Mechanical Engineering, Biomechanics Section, 3000 Leuven, Belgium

<sup>2</sup>University Hospital Leuven, Department of Orthopaedics, 3000 Leuven, Belgium

<sup>3</sup>KU Leuven, Department of Mechanical Engineering, LMSD Section, 3000 Leuven, Belgium

CORRESPONDING AUTHOR: Q. GOOSSENS (quentin.goossens@kuleuven.be)

This work was supported in part by IWT (Agency for Innovation by Science and Technology), Flanders, under Grant SB 81092; and in part by Internal Funds KU Leuven.

**ABSTRACT** Objective: The level of primary implant fixation in cementless total hip arthroplasty is a key factor for the longevity of the implant. Vibration-based methods show promise for providing quantitative information to help surgeons monitor implant fixation intraoperatively. A thorough understanding of what is driving these changes in vibrational behavior is important for further development and improvement of these methods. Additionally, an instrument must be designed to enable surgeons to leverage these methods. This study addresses both of these issues. Method: An augmented system approach was used to develop an instrument that improves the sensitivity of the vibrational method and enables the implementation of the necessary excitation and measurement equipment. The augmented system approach took into account the dynamics of the existing bone-implant system and its interaction with the added instrument. Results: Two instrument designs are proposed, accompanied by a convergence-based method to determine the insertion endpoint. The modal strain energy density distribution was shown to affect the vibrational sensitivity to contact changes in certain areas. Conclusion: The augmented system approach led to an instrument design that improved the sensitivity to changes in the proximal region of the combined bone-implant-instrument system. This fact was confirmed both *in silico* and *in vitro*. Clinical Impact: The presented method and instruments address practical intraoperative challenges and provide perspective to objectively support the surgeon's decision-making process, which will ensure optimal patient treatment.

**INDEX TERMS** Total hip arthroplasty, numerical and experimental modal analysis, femoral implant fixation assessment.

## I. INTRODUCTION

A surgeon's ability to consistently ensure optimal initial intraoperative implant stability for his or her patients is crucial to assure satisfactory long-term fixation of primary and revision femoral implants in cementless total hip arthroplasty (THA) [1]. Previous research [2]–[6] has shown that vibration methods are sensitive to changes that occur between bone and implant when contact is established during the insertion of the implant into the bone. These non-destructive vibration techniques have their origin in civil engineering where they are referred to as Structural Health Monitoring (SHM) techniques [7]. To bring these SHM techniques to assess the intraoperative primary fixation of cementless femoral implants to

clinical practice, a combined instrument has been developed. This instrument must be designed to attach to the implant and dynamically excite and measure the vibrational behavior of the bone-implant system. Previous studies explored some prototypes or methods to acquire the vibrational signature of a bone implant system. Tijou *et al.* [8] presents a vibrational force feature to assess femoral stem fixation in bone mimicking phantoms. Other existing prototypes have a number of practical limitations: they have a bulky design [2], need technical assistance to perform the excitation [3] or require modification of the implant [4]. Most comprise a mechanism to attach the instrument to the implant ('connector') and a part on which actuation and acquisition

can be performed (‘subsystem’). Goossens *et al.* [5] investigated the sound that resulted from insertion hammer blows to monitor femoral implant seating. This article presents an alternative approach in which a non-destructive vibration excitation was applied to the system in between insertion hammer blows, while contact-based sensors captured the response. The advantages of this approach over [5] are that it is repeatable and less affected by ambient airborne noise and operator variability. The first part of this study investigates the requirements for such an instrument and uses them to propose a proper shape for a femoral SHM instrument. The proposed designs aim to improve the vibrational performance of the method by adhering to a set of sensible guidelines deduced from mechanical insights into the bone-implant system. The second part of this study then verifies the performance of the proposed designs, both *in silico* and *in vitro*. The goal of this work is to develop a method and instrument to determine the insertion endpoint and thus provide a perspective to objectively support the surgeon’s intraoperative decision making. A brief summary of this work has been reported [9].

**II. METHODS AND PROCEDURES**

**A. DESIGN REQUIREMENTS AND PRINCIPLES**

The envisioned instrument aims to augment the vibrational sensitivity to important proximal bone-implant contact changes [10]–[12]. Also, to be used intraoperatively, it needs to fulfill a set of criteria concerning the practical usability of such an instrument. Table 1 presents an overview of the design criteria used during this work. This set of practical and technical requirements will need to be met by the instrument design and each aspect will be discussed in more detail in the following subsections. Since the key design principles that are presented in this paper focus on proximal femur-implant contact sensitivity, the presented instrument and method are generally applicable for primary cementless stems that rely on proximal fixation [10]–[12].

**TABLE 1. Overview of the instrument design requirements (Clinical Usability and SHM).**

Clinical Usability Requirements	SHM Requirements
- Free of interference (surgical work field & soft tissue)	- Vibrational sensitivity to proximal contact changes in damped conditions
- Biocompatible	- Dynamically coupled with the implant
- Convenient mounting to the implant	

**1) USABILITY REQUIREMENTS**

A key requirement for the envisioned intraoperative use is that the instrument can be seamlessly included into the surgical protocol. Based on the implant’s attachment location for surgical tools and the thickness of the patient’s soft tissue layer [13], a connector element with a length of 40 mm was devised that lead to an interference free design space for

the SHM instrument. The implant for which an instrument is developed in this work is the primary modular Profemur L cementless implant (Microport Orthopedics, Arlington, TN, USA). In order to simply mount and dismount the SHM instrument to the implant, the internal conical Morse taper with a M7 thread of the Profemur implant is used as slot for the instrument’s connector. Stainless steel (SS 316) is chosen as instrument material since it is biocompatible, used extensively in surgical instruments and has good sterilization properties [14].

**2) SHM REQUIREMENTS**

The addition of a SHM instrument to the bone-implant system results in an altered vibrational response of the augmented system. The use of additional substructures to passively modify the vibrational behavior of existing systems which were to be tested for damage was first proposed by [15] with the introduction of the concept of ‘twin’ structures for aerospace applications. Three main advantages of this approach exist. Firstly, with a good choice of twin structure, changes in the natural frequencies between the damaged and undamaged system can be amplified. Secondly, adding a subsystem increases the number of (sensitive) modes and frequencies of the system which may facilitate the damage identification process as more unknowns can be solved for in a model updating approach. Thirdly, addition of a subsystem leads to lowering of the natural frequencies of the combined system, which is desirable since lower frequencies are easier to measure. Several methods to generate these ‘twin’ structures are suggested; submerging, extending, embedding and changing the structure’s boundary conditions [15]. The methodological approach most suitable for the bone-implant system under study is to extend the bone-implant system to positively affect the performance of the SHM system. The main advantage of adding additional elements to an existing structure is that by implementing this modification the elastic strain energy distribution of the structure can be altered. It is theorized that the distribution of the elastic strain energy has an important influence on the detectability of a contact change in a particular zone. Therefore, changes in the critical proximal zone are only detectable in the higher frequency range. A higher frequency range typically exhibits higher modal damping, thereby reducing its contribution to the vibrational response. The following sections present the requirements that are used to design the instrument’s subsystem to optimize its vibrational performance. These requirements will incrementally further define the subsystem design space.

***a: MAXIMIZE VIBRATIONAL FEATURE SENSITIVITY FOR PROXIMAL CONTACT CHANGES IN DAMPED CONDITIONS***

The most fundamental challenge in SHM probably is the fact that damage typically is a local phenomenon and may not significantly influence the lower-frequency global response of a structure [7], except when damage is located near a region with high modal strain energy density (MSED). The crucial proximal region, located near the end of the bone-implant

system shows little strain for the first bending modes. Lower frequency modes however are generally easier to measure and are more limitedly influenced by damping. Nevertheless, the bone-implant system has the advantage that the system can be augmented to perform testing and thus by adding a structure to the system, the modal strain energy distribution of the system can be modified. Additionally, knowledge that the proximal region needs to be interrogated by the SHM system is an important advantage. Extending the system and in this manner modifying the modal strain energy distribution of the system is proposed by altering the geometrical structure of the system, which is a passive option that could be implemented realistically for the bone-implant system. The design goal is to change the elastic strain energy distribution of the augmented system so that the number of mode shapes which display high MSED values in the proximal region is increased (and thus will be sensitive to changes in this region) and that this region is interrogated by modes in a lower frequency range to mitigate the influence of damping. A simple numerical experiment is set up to illustrate the influence of geometrical changes to the system. To reduce the complexity inherently present when working with biomechanical constructs, consider the bending and longitudinal behavior of a bone-implant system to be approximated by a simple beam model (Fig. 3). For the results of this experiment, material properties nor geometry needed to correspond to those found for the bone-implant system. The model consists of 1000 linear beam elements, has a circular cross-section with a radius of 10 mm and a length of 1000 mm. Homogeneous material properties were chosen with an E-modulus of 100 GPa and a density of 4 g/cm<sup>3</sup>. The first 13 flexible modes were calculated which resulted in two longitudinal mode shapes (L1, L2) and 11 bending mode shapes (B1-B11) spanning a range up to 5000 Hz. In addition, the MSED was calculated for every mode shape. To establish a relation between changes to the system at certain locations and its effect on the resonance frequencies of the model, the stiffness of one element was reduced by 80% and the resonance frequencies of the altered model were calculated. Only one element was changed at a time, and its location was moved consecutively from the end of the beam model (at 0.1% of total length) towards the middle of the model (at 50% of total length) in 11 steps (at 0.1%, 5%, 10%, 15%, 20%, 25%, 30%, 35%, 40%, 45% and 50% of total length). The results and findings of this simulation are presented in III-A.1.

#### *b: ENSURE DYNAMIC COUPLING BETWEEN IMPLANT AND INSTRUMENT*

The results corresponding to previous sections sketched some design bounds for the development of the shape of the instrument's subsystem. In order to converge towards a specific design, an additional consideration is taken into account. Every instrument and subsystem design should ensure that changes to the vibrational behavior of the implant are observable on the instrument. This means that the

implant-instrument vibrational behavior should be well coupled and that the deformation of the system's mode shapes are global, rather than local. Local, uncoupled behavior of the subsystem may lead to a vibrational response that is dominated by the local deformation patterns of the subsystem and is decoupled from changes in vibrational behavior of the implant it is intended to make observable. A simple, albeit not the only criterion to ensure proper coupling is by adding a subsystem which has a mechanical impedance close to the system it couples to. Analogous to electrical systems, matched impedance systems facilitate an easy transfer of energy within the system [16]. The dynamic impedance of mechanical structures is mainly characterized by the structure's resonance frequencies. A free-free finite (FE) simulation of the Profemur size five and size six implant with only the connector (manufactured from stainless steel,  $E = 210$  GPa,  $\rho = 7.9$  g/cm<sup>3</sup>) attached was performed to determine the first bending modes. These resonance frequencies were used to shape the instrument to match the frequencies of the implant-connector system. A closed analytical formula [17] is available providing the resonance frequencies of a beam given its dimensions and boundary conditions. This allows us to precisely match these first resonance frequencies in both directions by modifying the length, width and height of this beam structure. To determine three parameters given two resonance frequencies conditions, one can be chosen freely. The width of the beam is set at 9 mm to provide sufficient space for standard off-the-shelf measurement and excitation equipment. The corresponding results and selected instrument designs are presented in III-A.2. Following the selection of two instrument designs, free-free FE simulations of the combined implant-instrument systems were performed. This analysis was performed to assess the dynamic coupling between the implant and the instrument. Titanium alloy ( $E = 105.8$  GPa,  $\rho = 4.33$  g/cm<sup>3</sup>) and stainless steel material properties were used for the implant and instruments respectively. Section III-A.2 presents the results of this analysis.

#### **B. IN SILICO STUDY**

In order to assess the performance of the two instrument designs, FE models were built comprising bone, implant and instrument. The vibrational behavior of these bone-implant-instrument models was contrasted to the vibrational behavior of a reference bone-implant model. The FE models were built from a CT-scanned replicate femur model (size medium, Sawbones, Vashon Island, WA, USA) and a 3D scanned Profemur L cementless femoral stem (size 6, Microport Orthopedics, Arlington, TN, USA). The models are depicted in Fig. 1. Bone material properties were assigned according to [18] in which the femur model was validated using *in vitro* experimental results. Titanium alloy material properties were assigned to the implant and stainless steel properties were assigned to the instruments. Nodes of implant and bone model within a distance of 0.005 mm were merged to simulate a fully bonded interface [19]. A mesh convergence analysis

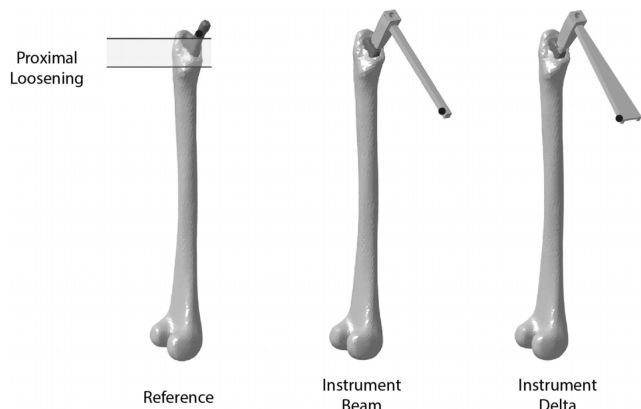


**FIGURE 1.** Illustration of the three FE models used in the *in silico* experiment. The proximal zone (first third of the bone-implant contact zone) that is loosened in the numerical experiment is highlighted for the reference implant model.

was performed for all FE models to determine the appropriate element size. The final bone-implant model consisted of 63319 quadratic tetrahedral elements and was validated by experimental results from a corresponding *in vitro* model. The instrument-beam and instrument-delta model consisted of 30209 and 76370 quadratic tetrahedral elements respectively. Two cases were simulated using these models. The first case considers the implant to be in full contact with the bone, the second case assumes a loss of contact in the proximal region, corresponding to the first third of the bone-implant contact zone (Fig. 1). Numerous studies have shown that the proximal contact area has the most effect on primary stability of cementless implants [10]–[12], so any SHM instrument aiming to improve the surgeon’s decision-making process during surgery should demonstrate high sensitivity to contact changes in this area. A modal analysis was performed on all models in the 10-10000 Hz range. A set of direct frequency response functions (FRFs) was synthesized at the virtual measurement points in the AP direction (Fig. 1) with a frequency resolution of one Hz. The FRFs of the two cases were compared using the Pearson’s correlation (PC) metric:

$$PC = \frac{\sum_{\omega=a}^b (|H(\omega)|_{N-1} - \overline{|H(\omega)|_{N-1}})(|H(\omega)|_N - \overline{|H(\omega)|_N})}{\sqrt{\sum_{\omega=a}^b (|H(\omega)|_{N-1} - \overline{|H(\omega)|_{N-1}})^2} \sqrt{\sum_{\omega=a}^b (|H(\omega)|_N - \overline{|H(\omega)|_N})^2}} \quad (1)$$

where  $|H(\omega)|_{N-1}$  is the FRF magnitude measured at insertion step N-1.  $|H(\omega)|_N$  is the FRF magnitude measured and excited at the same locations for insertion step N. The PC is calculated in a frequency range from a to b.

The PC is a dimensionless index that ranges from -1.0 to 1.0 and reflects the extent of a linear relationship between two data sets. To understand the influence of including higher frequency information on the metric, PC values were calculated for ranges spanning 100-750 Hz to 100-10000 Hz with 1 Hz increments. Mechanical damping properties of

the bone-implant construct have an important effect on the shape of the FRF and thus on how frequency changes in the underlying system are reflected in this feature. To understand the influence modal damping has on the sensitivity of the FRF feature to contact changes, several modal damping scenarios were assumed for both cases. The scenarios with a modal damping of 0.5%, 1.5% (composite bone models [18]), 5% (cadaveric bone models [20]) and 10% (extreme case) were considered to be the same for all modes in the 10–10000 Hz frequency range. Additionally, a scenario was added with 2.5% in the 10–2000 Hz range and 4.5% in the range above 2000 Hz. This variation in modal damping with lower damping coefficients in the low frequency range and higher modal damping in the higher frequency range corroborates better with the experimental findings of a cadaveric pilot study.

### C. IN VITRO STUDY

Next, the performance of both instrument designs was verified by an *in vitro* experiment. The two instrument designs were manufactured using wire EDM (GF cut 300ms, AgieCharmilles, Geneva, Switzerland) and CNC milling (Kern Evo, Kern Microtechnik GmbH, Eschenlohe, Germany) from stainless steel alloy (SS 316). A composite femur model (Sawbones model 3403 (size medium), Sawbones Europe AB, Malmö, Sweden) was prepared by an experienced surgeon for implantation of an uncemented Profemur L size five implant using manufacturer provided standard instruments. After preparation, the implant was hammered in by the surgeon. After every insertion step, the subsidence of the implant was measured using a caliper. Three FRFs were collected after every insertion step; one on the bone-implant system (proximal edge of the Profemur implant), one on the system with the instrument-beam design mounted and one on the system with the instrument-delta design mounted. This allowed us to compare and contrast the evolution of the FRF feature for the different systems. The measurement points on the instruments corresponded to the measurement points used in the *in silico* experiment. All FRFs were acquired in the AP direction. The excitation was performed by impact using a modal hammer (086C03, PCB Piezotronics, Depew, NY, USA) and the acceleration response was measured using a lightweight accelerometer (A352A24, PCB Piezotronics, Depew, NY, USA). Data acquisition and conditioning was performed using a spectral analyzer (Simcenter SCADAS Mobile, Siemens PLM Software, Leuven, Belgium) and corresponding software (Simcenter Testlab, Siemens PLM Software, Leuven, Belgium). The sampling frequency was set to 20.48 kHz, the frequency resolution was 0.625 Hz. Data processing was performed in Matlab (MathWorks, Natick, MA, USA). Free-free conditions were simulated to mimic the *in vivo* situation [21].

Fig. 2 shows the bone-implant systems without and with the instruments mounted. In addition to comparing the change in the FRFs using the PC an additional metric

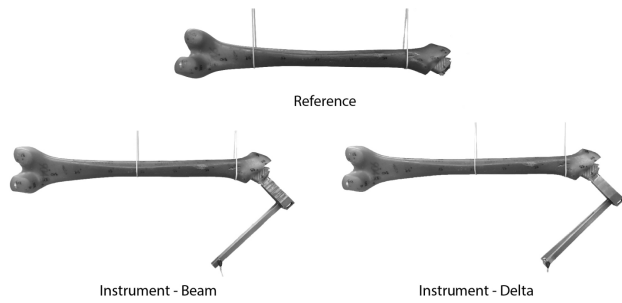


FIGURE 2. The three experimental model configurations tested.

is introduced, the Frequency Response Assurance Criterion (FRAC). Corollary to the MAC used for mode shape comparison, the FRAC operates on the complex FRF vector rather than on the FRF magnitude as is the case for the PC.

$$FRAC = \frac{\left| \sum_{\omega=a}^b H(\omega)_{N-1} H^*(\omega)_N \right|^2}{\sum_{\omega=a}^b H(\omega)_{N-1} H^*(\omega)_{N-1} \sum_{\omega=a}^b H(\omega)_N H^*(\omega)_N} \quad (2)$$

where  $H(\omega)_{N-1}$  is the FRF measured at insertion step N-1.  $H(\omega)_N$  is the FRF measured and excited at the same locations for insertion step N. The FRAC is calculated in a frequency range from a to b.

### III. RESULTS AND DISCUSSION

#### A. DESIGN REQUIREMENTS AND PRINCIPLES

##### 1) SHM REQUIREMENTS: MAXIMIZE VIBRATIONAL FEATURE SENSITIVITY FOR PROXIMAL CONTACT CHANGES IN DAMPED CONDITIONS

This paragraph presents the results of the simplified numerical beam model as described in section II-A.2. The effect of the applied change in stiffness on the resonance frequencies is provided in the table in Fig. 3. In accordance with literature [7], resonance frequency changes are low despite a 80% local change in stiffness. In spite of this, the results again confirm that when a stiffness change is applied in a region close to a region with an elevated MSED for a particular mode, the change in resonance frequency of that mode is larger. The closer the change is applied to the region around 50% of total length, the lower the frequencies that are affected. Also, the number of frequencies that are sensitive to a stiffness change increases as the location of the defect moves from the edge towards the middle of the beam system. Considering a threshold at 0.15% to flag a frequency as sensitive to the local change (which corresponds approx. to half of the maximum resonance frequency percentage change), an important increase of the number of sensitive resonance frequencies is observed when the change is present around the 10-15% of total length region. Fig. 4 translates the findings of this simulation to the femoral bone-implant system. The

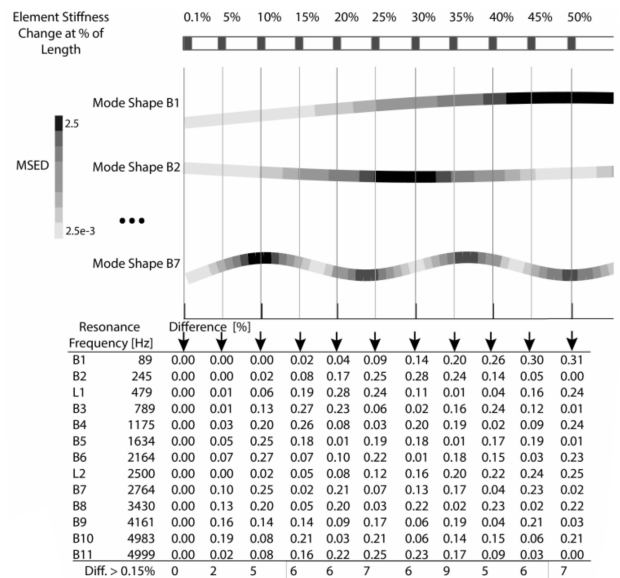


FIGURE 3. Illustration of the deformed bending (B) and longitudinal (L) mode shapes and corresponding MSED distribution of a simplified beam model. The location where the element stiffness was changed, was consecutively altered from a position located at 0.1% of total length to a position at 50% of total length. The table presents the percentage change for the first 13 resonance frequencies. The first column of this table for example lists the frequency changes for the 80% stiffness reduction in the element located at 0.1% of total length.

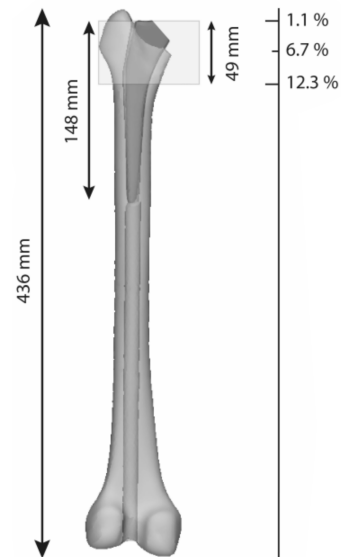


FIGURE 4. The relative positioning of the calcar zone (at 6.7%) and the full proximal zone.

configuration depicted presents the geometry of a Sawbones composite femur model in combination with a Profemur size five implant. The crucial calcar zone is at 6.7% of total length and thus outside of the more sensitive region as was found for the beam model. Based on the simplified model, the region above the calcar zone is expected to be very little

influenced by stiffness changes in the system (e.g., due to contact changes), whereas the region below is expected to be more sensitive. The total proximal zone comprises approx. 10% of the total length of the bone. To increase the number of resonance frequencies sensitive to a change in contact, the calcar zone should be located at between 15% and 50% of the total length. Considering the length of 40 mm of the connector, this observation leads to a definition of a relative length range of the subsystem so that it puts the calcar zone between 15% and 50% of the total length of the combined system. It is important to notice that this is an estimate of the length that can be added, as this discards any possible geometrical stiffening effects due to the shape of the instrument as compared to a straight beam assumption as was used for this numerical experiment.

## 2) SHM REQUIREMENTS: ENSURE DYNAMIC COUPLING BETWEEN IMPLANT AND INSTRUMENT

The first bending mode of the implant-connector structure is found at an average resonance frequency of 1898 Hz in the antero-posterior (AP) direction and 1928 Hz in the medio-lateral (ML) direction. A first straightforward design would be to shape the subsystem as a beam with rectangular cross section. Given the width (9mm), the length and height of the beam were solved to be 158 mm and 9.14 mm respectively to match the first AP and ML bending modes of the implant-connector. With a total instrument length of 198 mm, the calcar zone would thus be located at 36% from the top, which puts it comfortably in the sensitive target region as defined in the previous section. This approach leads to a shape of instrument which is very similar in size to the implant as it is in weight. A second design adopted a delta shape for the subsystem. The length of the subsystem as well as the height is kept the same for this design, but the width is changed. Rather than increasing the width of the beam over the whole length, a delta approach allowed us to investigate the influence of an increased stiffness in one direction without adding an excessive amount of weight. With a width of 30 mm at the wide end of the delta shape, its first bending frequency in the AP direction was 3657 Hz which is close to the second AP bending mode resonance frequency of the implant-connector at 3616 Hz. Both designs are depicted in Fig. 5. Fig. 5 also illustrates the first and second bending mode shapes of the combined implant-instrument models. The modal deformation shows that the design goal to develop an implant-instrument combination that is well coupled and shows global rather than local bending deformation patterns is well met by both designs. The similarity in impedance in the ML direction is substantiated by the closeness of their respective resonance frequencies, contrary to the bending behavior in the AP direction where the resonance frequencies, in particular for the second bending mode, are raised due to the increased design stiffness in this direction. It is of interest to consider that for other bone lengths, this same length

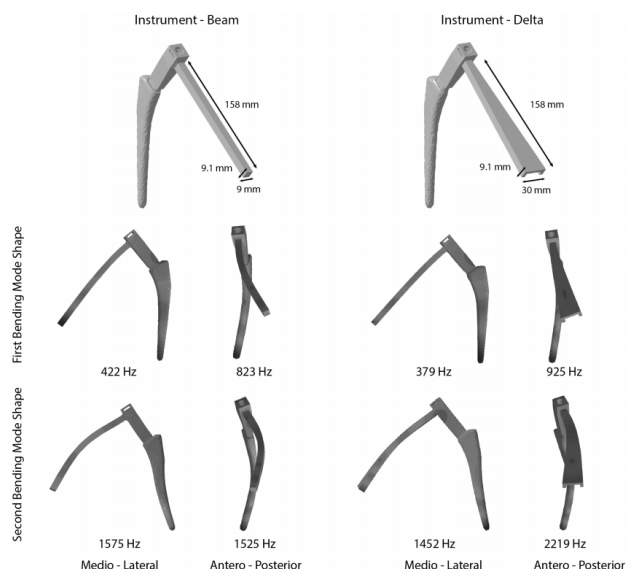


**FIGURE 5.** Both instrument designs adhering to the full set of requirements and their first and second bending modes are depicted.

addition positions the calcar zone at 38.9% (bone length of 375 mm) and at 33.9% (bone length of 482 mm). For a wide range of bone sizes, this length addition thus ensures positioning the calcar zone in a sensitive MSED region.

## B. IN SILICO STUDY

### 1) BONE-IMPLANT-INSTRUMENT MODEL

The results of the *in silico* experiment are presented in Fig. 6 for the three different models. The figure comprises the following parts: the upper figures show the synthesized FRFs for a fully fixed and proximal loosened model with the 2.5%-4.5% modal damping scenario for the three configurations. The figures below the FRFs show the metric values (PC) indicating the feature's difference between a fully fixed and proximal loosened case. The metric values are calculated and plotted for varying ranges. E.g., the PC value plotted at 2000 Hz is the PC value calculated between the two fixation cases in the 100-2000 Hz range. Similarly, the value plotted at 4000 Hz is the PC value obtained for the 100-4000 Hz range etc. Rather than relying on a single PC value for a certain range, this representation gives insight into the sensitivity of the metric to the selected range. Lower values indicate higher sensitivity to contact changes in this area. In general, the metric values obtained for the implant-instrument combinations are importantly lower than those of the reference model, except for the scenario with the lowest modal damping (0.5%). Including the higher frequency range into the metric for the reference model improves the sensitivity of the metric, however this becomes less influential as damping increases.

This increased higher frequency sensitivity is in accordance to previous findings [22]. Although damping also

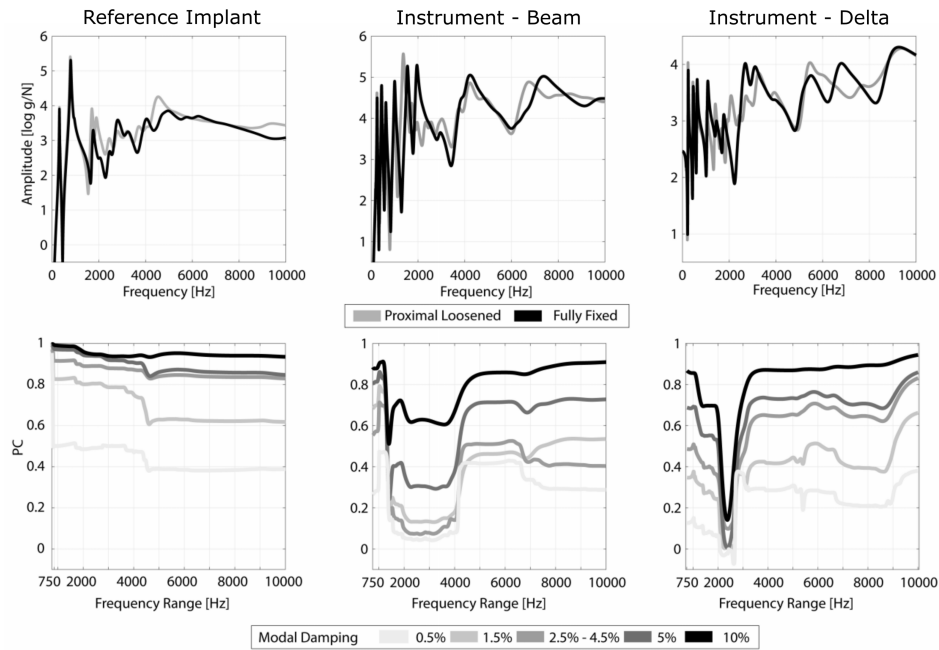


**FIGURE 6.** Results of the *in silico* experiment: the upper graphs present the proximal loosened and fully fixed FRF amplitudes for the three configurations (reference, instrument-beam and instrument-delta) with 2.5%-4.5% damping. The lower graphs present the PC metric calculated between the proximal loosened and fully fixed FRF's that are plotted above. The PC metrics are presented as function of the upper frequency limit (x-axis).

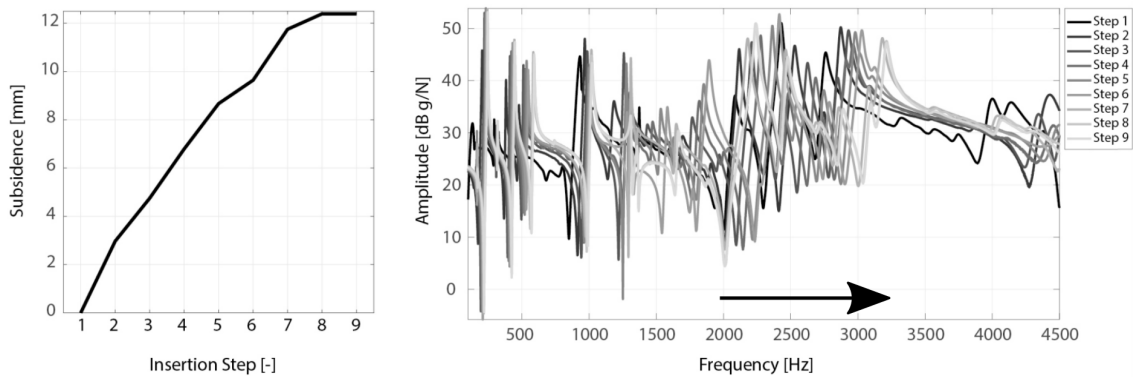


**FIGURE 7.** The implant was hammered in with 8 hammer blows subsiding 12.2 mm. The FRF amplitude graphs illustrate the change in vibrational behavior as the insertion process progresses. The FRF's clearly shift over the entire frequency range. More specific, a noticeable shift is visible around 2500 Hz as marked by the arrow.

affects the sensitivity of the implant-instrument models, adequate performance of the metric is still expected to be present even in highly damped conditions and especially in the lower frequency region. The instrument-delta design has better low frequency performance and lower minimal values than the instrument-beam design when the range is extended to 2500 Hz, however the instrument-beam design shows lower swings in sensitivity across the full frequency range. The presence of more resonance frequencies (15 resonance frequencies in the 10-3000 Hz range for both instrument models versus eight for the reference model) sensitive to changes in the proximal contact region observable in the

FRF offers an explanation for the decrease of metric values observed. Table 2 summarizes these results. In summary, the two instruments demonstrated their expected behavior in this *in silico* study. The next section illustrates how this numerical performance is translated to an experimental setting.

### C. IN VITRO STUDY

This section presents the results of the *in vitro* verification of the instrument designs. Fig. 7 shows the evolution of the implant subsidence and, as an example, shows the FRFs for all steps of the instrument-delta configuration. To compare the FRF evolution between the different configurations,

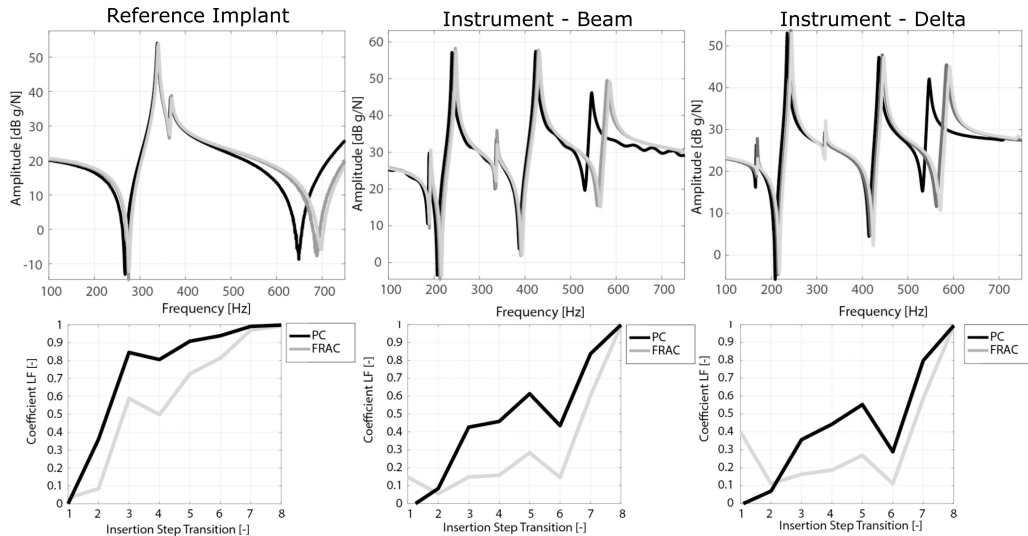


**FIGURE 8.** FRF amplitudes of steps six to eight in a range of 100-750 Hz and metric values (PC and FRAC) calculated on the same range are shown for all three experimental configurations.

**TABLE 2.** Summary of the numerical experiment results. The mean (standard deviation), maximal and minimal PC values are calculated on the 100-10000 Hz range. The mean (standard deviation) value is calculated for the 100-1000 Hz range.

Reference					
Modal Damping	0.5%	1.5%	2.5/4.5%	5.0%	10.0%
<i>PC 10000 Hz Range</i>					
Mean	0.43	0.69	0.86	0.89	0.95
(SD)	(0.06)	(0.09)	(0.03)	(0.04)	(0.02)
Max	0.95	0.97	0.99	1.00	1.00
Min	0.38	0.61	0.83	0.84	0.93
<i>PC 1000 Hz Range</i>					
Mean	0.58	0.85	0.93	0.98	0.99
(SD)	(0.16)	(0.05)	(0.03)	(0.01)	(0.00)
Instrument - Beam					
Modal Damping	0.5%	1.5%	2.5/4.5%	5.0%	10.0%
<i>PC 10000 Hz Range</i>					
Mean	0.27	0.36	0.40	0.60	0.80
(SD)	(0.14)	(0.18)	(0.17)	(0.18)	(0.11)
Max	0.47	0.71	0.79	0.86	0.91
Min	0.04	0.07	0.13	0.24	0.51
<i>PC 1000 Hz Range</i>					
Mean	0.28	0.58	0.70	0.82	0.88
(SD)	(0.03)	(0.02)	(0.02)	(0.01)	(0.01)
Instrument - Delta					
Modal Damping	0.5%	1.5%	2.5/4.5%	5.0%	10.0%
<i>PC 10000 Hz Range</i>					
Mean	0.23	0.40	0.59	0.66	0.81
(SD)	(0.10)	(0.14)	(0.16)	(0.17)	(0.17)
Max	0.38	0.66	0.83	0.86	0.94
Min	-0.07	-0.05	0.10	0.00	0.14
<i>PC 1000 Hz Range</i>					
Mean	0.13	0.35	0.49	0.69	0.86
(SD)	(0.01)	(0.01)	(0.00)	(0.00)	(0.01)

Fig. 8 illustrates the FRFs of steps six to eight of the insertion process for the reference, instrument-beam and instrument-delta experiments in a range of 100-750 Hz to focus on the

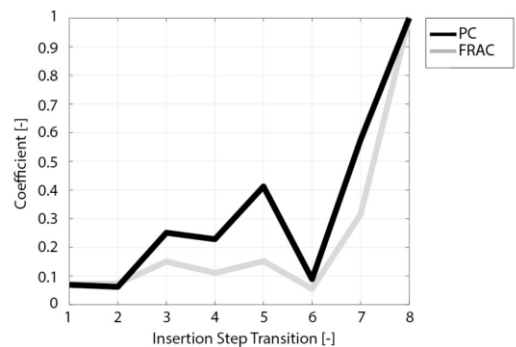


**FIGURE 9.** Both the PC and FRAC metric decreased importantly when a range up to 2500 Hz was selected using the instrument-delta design.

low frequency (LF) behavior. The PC and FRAC metrics obtained by comparing the FRFs of subsequent steps are presented for all three configurations, the metric was calculated in the 100-750 Hz range, thus making it possible to assess the influence and sensitivity of the low frequency vibrational behavior to the insertion process. The first five instrument-beam FRAC and PC metrics are on average respectively lower by an amount of 0.23 and 0.27 compared to the reference configuration. These differences are even more important for the metric values at six and seven, with FRAC values lower by an amount of 0.67 and 0.37 and the PC values lower by an amount of 0.50 and 0.15. Similarly, the first five instrument-delta metric values were lower by an average of 0.16 (FRAC) and 0.30 (PC) compared to the reference configuration. Metric values at steps six and seven were lower by 0.70 and 0.41 (FRAC) and by 0.65 and 0.20 (PC) compared to the reference configuration. The high metric values obtained for the reference configuration make discerning between the last few steps difficult. In contrast, the low values obtained for the instrument-augmented configurations make it possible to

easily discriminate between the penultimate and the ultimate step. The clear shift of the third mode in the low frequency region reflects the modified strain distribution that the addition of the instrument causes to the bone-implant system, as was its design intent. The choice of metric influences the information extracted by the method. Ideally, the differences reflected in the metric are as high as possible as long as the implant has not reached its final position and close to zero when the final position is reached. The FRAC metric values obtained were generally lower than the PC metric values in the steps leading up to the insertion endpoint and were comparable at insertion endpoint. Values for both were above 0.99 at the insertion endpoint. The 0.99 threshold was proposed in previous research for the PC metric [3], [22], but also seems a proper threshold for the FRAC metric. Exploiting the richer information content available by processing the complex vectors as compared to only comparing one dimension of those same FRFs thus seems to be advantageous at most steps, without changing the insertion endpoint threshold value. Two additional observations are interesting to point out. Firstly, the numerical study indicated a very sensitive region around 2500 Hz for the instrument-delta design with an important shift of the resonance frequency when proximal contact was established. This same behavior is visible in the experimental measurements when the FRFs for the instrument-delta design for steps six, seven and eight are investigated in the 2000-2500 Hz range (Fig. 7). This confirms the assumption that proximal contact is established in the final steps of the insertion process and confirms the relevance of the numerical cases simulated. Secondly, the sensitivity of the metric was shown to increase importantly when this region was included in the numerical study. When the instrument-delta design metrics are calculated for the range 100-2500 Hz, the metric values indeed are considerably lower, indicating an increased sensitivity to changes during the insertion process (Fig. 9).

Summarizing the experimental findings, it was shown that the instrument augmented systems adequately interrogate the proximal region of the bone-implant system. The increased sensitivity towards the end of the insertion allows for a better differentiation between the penultimate and end step and thus for a better estimation of the insertion endpoint. The vibrational behavior in the low frequency region proved sensitive to proximal changes, which is especially of interest when damping in the system would increase. The observed behavior of the FRF and the similarity to the simulated cases furthermore confirms that proximal contact is indeed made in the last steps of the insertion process. Comparing the two instrument designs, although both designs show adequate performance compared to the reference configuration, it was found that the instrument-delta design was a bit more sensitive in the low frequency region.

#### IV. CONCLUSION

This article presents the design of two instruments that could be attached to a cementless THA implant as a part of

a non-destructive method to assess fixation in real-time. A set of requirements were proposed to guide this design. The instruments were developed to modify the modal strain energy distribution of the augmented system to increase the sensitivity of the bone-implant system to proximal contact changes. The performance of the design was verified numerically. The effects of the modified strain distribution were visible in the decreased metric values and amongst other effects showed an increase of the sensitivity in the low frequency range, which is less prone to damping influences. The instrument designs were manufactured and tested *in vitro*. The *in vitro* results correlated well to the numerical experiments. Although the performance of both designs was similar, the instrument-delta design was chosen as the prime candidate for subsequent cadaveric testing as the low frequency sensitivity was slightly better. The designs presented are not the only solution adhering to the guidelines, but experiments showed how an auxiliary subsystem could be used to impact the vibrational behavior of the bone-implant system. An additional metric (FRAC) was proposed to compare subsequent FRFs and the threshold for both metrics was set at 0.99. The presented method and instruments address the practical intraoperative challenges and provide perspective to objectively support the surgeon's decision-making process to ensure optimal patient treatment.

#### REFERENCES

- [1] M. Viceconti, A. Pancanti, E. Varini, F. Traina, and L. Cristofolini, "On the biomechanical stability of cementless straight conical hip stems," *Proc. Inst. Mech. Eng., H, J. Eng. Med.*, vol. 220, no. 3, pp. 473–480, Mar. 2006, doi: [10.1243/09544119H06904](https://doi.org/10.1243/09544119H06904).
- [2] E. Varini, E. Bialoblocka-Juszczak, M. Lannocca, A. Cappello, and L. Cristofolini, "Assessment of implant stability of cementless hip prostheses through the frequency response function of the stem–bone system," *Sens. Actuators A, Phys.*, vol. 163, no. 2, pp. 526–532, Oct. 2010, doi: [10.1016/j.sna.2010.08.029](https://doi.org/10.1016/j.sna.2010.08.029).
- [3] L. C. Pastrav, S. V. N. Jaecques, I. Jonkers, G. Van der Perre, and M. Mulier, "In vivo evaluation of a vibration analysis technique for the per-operative monitoring of the fixation of hip prostheses," *J. Orthopaedic Surg. Res.*, vol. 4, no. 1, p. 10, Dec. 2009, doi: [10.1186/1749-799X-4-10](https://doi.org/10.1186/1749-799X-4-10).
- [4] A. Crisman, N. Yoder, M. McCuskey, M. Meneghini, and P. Cornwell, "Femoral component insertion monitoring using human cadaveric specimens," in *Proc. 25th IMAC Conf. Struct. Dyn.*, 2007, pp. 1–15.
- [5] Q. Goossens *et al.*, "Acoustic analysis to monitor implant seating and early detect fractures in cementless THA: An *in vivo* study," *J. Orthopaedic Res.*, vol. 39, no. 6, pp. 1164–1173, Jun. 2021, doi: [10.1002/jor.24837](https://doi.org/10.1002/jor.24837).
- [6] H. A. Lomami *et al.*, "Ex vivo estimation of cementless femoral stem stability using an instrumented hammer," *Clin. Biomech.*, vol. 76, Jun. 2020, Art. no. 105006, doi: [10.1016/j.clinbiomech.2020.105006](https://doi.org/10.1016/j.clinbiomech.2020.105006).
- [7] C. R. Farrar and K. Worden, *Structural Health Monitoring: A Machine Learning Perspective*. Hoboken, NJ, USA: Wiley, 2013.
- [8] A. Tijou *et al.*, "Monitoring cementless femoral stem insertion by impact analyses: An *in vitro* study," *J. Mech. Behav. Biomed. Mater.*, vol. 88, pp. 102–108, Dec. 2018, doi: [10.1016/j.jmbbm.2018.08.009](https://doi.org/10.1016/j.jmbbm.2018.08.009).
- [9] Q. Goossens *et al.*, "Development of a femoral implant instrument to assess primary stability using vibrational analysis," presented at the 25th Congr. Eur. Soc. Biomech. (ESB), Vienna, Austria, 2019.
- [10] M. Reimeringer, N. Nuño, C. Desmarais-Trépanier, M. Lavigne, and P. A. Vendittoli, "The influence of uncemented femoral stem length and design on its primary stability: A finite element analysis," *Comput. Methods Biomech. Biomed. Eng.*, vol. 16, no. 11, pp. 1221–1231, Nov. 2013, doi: [10.1080/10255842.2012.662677](https://doi.org/10.1080/10255842.2012.662677).

- [11] F. H. Dujardin, R. Mollard, J. M. Toupin, A. Coblenz, and J. M. Thomine, "Micromotion, fit, and fill of custom made femoral stems designed with an automated process," *Clin. Orthopaedics Rel. Res.*, vol. 325, pp. 276–289, Apr. 1996, doi: [10.1097/00003086-199604000-00034](https://doi.org/10.1097/00003086-199604000-00034).
- [12] P. O. Østbyhaug, J. Klaksvik, P. Romundstad, and A. Aamodt, "Primary stability of custom and anatomical uncemented femoral stems," *Clin. Biomech.*, vol. 25, no. 4, pp. 318–324, May 2010, doi: [10.1016/j.clinbiomech.2009.12.012](https://doi.org/10.1016/j.clinbiomech.2009.12.012).
- [13] S. Jain, A. Lahoti, K. Pandey, and P. Rao, "Evaluation of skin and subcutaneous tissue thickness at insulin injection sites in Indian, insulin naïve, type-2 diabetic adult population," *Indian J. Endocrinol. Metabolism*, vol. 17, no. 5, p. 864, 2013, doi: [10.4103/2230-8210.117249](https://doi.org/10.4103/2230-8210.117249).
- [14] D. L. Bartel, D. T. Davy, and T. M. Keaveny, *Orthopaedic Biomechanics?: Mechanics and Design in Musculoskeletal Systems*. London, U.K.: Pearson, 2006.
- [15] P. Trivailo, L. Plotnikova, and L. Wood, "Enhanced parameter identification for damage detection in aerospace structures using 'twin' structures concept," presented at the ICSV, 1997.
- [16] T. L. Floyd, *Principles of Electric Circuits*. Upper Saddle River, NJ, USA: Prentice-Hall, 2000.
- [17] A. Shabana, *Vibration of Discrete and Continuous Systems*. New York, NY, USA: Springer, 1997.
- [18] S. Leuridan *et al.*, "Determination of replicate composite bone material properties using modal analysis," *J. Mech. Behav. Biomed. Mater.*, vol. 66, pp. 12–18, Feb. 2017, doi: [10.1016/j.jmbbm.2016.10.018](https://doi.org/10.1016/j.jmbbm.2016.10.018).
- [19] C. Dopico-González, A. M. New, and M. Browne, "Probabilistic finite element analysis of the uncemented hip replacement—Effect of femur characteristics and implant design geometry," *J. Biomech.*, vol. 43, no. 3, pp. 512–520, Feb. 2010, doi: [10.1016/j.jbiomech.2009.09.039](https://doi.org/10.1016/j.jbiomech.2009.09.039).
- [20] B. Couteau, M.-C. Hobatho, R. Darmana, J.-C. Brignola, and J.-Y. Arlaud, "Finite element modelling of the vibrational behaviour of the human femur using CT-based individualized geometrical and material properties," *J. Biomech.*, vol. 31, no. 4, pp. 383–386, Apr. 1998, doi: [10.1016/S0021-9290\(98\)00018-9](https://doi.org/10.1016/S0021-9290(98)00018-9).
- [21] G. van der Perre and G. Lowet, "In vivo assessment of bone mechanical properties by vibration and ultrasonic wave propagation analysis," *Bone*, vol. 18, no. 1, pp. S29–S35, Jan. 1996, doi: [10.1016/8756-3282\(95\)00377-0](https://doi.org/10.1016/8756-3282(95)00377-0).
- [22] L. C. Pastrav, S. V. N. Jaecques, M. Mulier, and G. Van der Perre, "Detection of the insertion end point of cementless hip prostheses using the comparison between successive frequency response functions," *J. Appl. Biomater. Biomech.*, vol. 6, no. 1, pp. 23–29, Jan. 2008.